REVIEW

National Science Review
4: 224–239, 2017
doi: 10.1093/nsr/nww024
Advance access publication 19 April 2016

CHEMISTRY

Organic light-emitting diodes: theoretical understanding of highly efficient materials and development of computational methodology

Zhigang Shuai[1,2,*] and Qian Peng[2,*]

ABSTRACT

Theoretical understanding of organic light-emitting diodes started from the quest to the nature of the primary excitation in organic molecular and polymeric materials. We found the electron correlation strength, bond-length alternation as well as the conjugation extent have strong influences on the orderings of the lowest lying excited states through the first application of density matrix renormalization group theory to quantum chemistry. The electro-injected free carriers (with spin 1/2) can form both singlet and triplet bound states. We found that the singlet exciton formation ratio can exceed the conventional 25% spin statistics limit. We proposed a vibration correlation function formalism to evaluate the excited-state decay rates, which is shown to not only give reasonable estimations for the quantum efficiency but also a quantitative account for the aggregation-induced emission (AIE). It is suggested to unravel the AIE mechanism through resonance Raman spectroscopy.

Keywords: excited-state theory, organic electroluminescence, spin statistics, quantum efficiency, vibration correlation function

[1]MOE Key Laboratory of Organic Optoelectronics and Molecular Engineering, Department of Chemistry, Tsinghua University, Beijing 100084, China and [2]CAS Key Laboratory of Organic Solids, Institute of Chemistry, Chinese Academy of Sciences, Beijing 100190, China

*Corresponding authors. E-mails: zgshuai@tsinghua.edu.cn; qpeng@iccas.ac.cn

Received 6 January 2016; **Revised** 29 February 2016; **Accepted** 29 February 2016

INTRODUCTION

The electro-pumped organic molecular film can be made by highly efficient light-emitting devices, as discovered by Tang and van Slyke [1] for small molecules and by Burroughes *et al.* for polymers [2]. Gustaffson *et al.* proposed solution-processed printable polymer light-emitting technology [3]. Later, Ma and Che *et al.* [4] and Thompson and Forrest *et al.* [5] expanded materials system to organometallic molecules to promote the internal light-emitting quantum efficiency by utilizing the electro-pumped triplet states with the aid of the strong spin–orbit coupling. And then, to avoid severe triplet–triplet annihilation (TTA), organometallic dendrimers have been suggested to get rid of the efficiency drooping at high current intensity [6]. In the typical electroluminescent device, charge carriers (electrons and holes) are injected into the active layer to form both singlet and triplet bound pairs in addition to electric current (waste). The overall external quantum efficiency can be written as: $\eta = \eta_{\rm rec}\eta_{\rm S}\eta_{\rm pl}\eta_{\rm OC}$, where $\eta_{\rm rec}$ is the recombination ratio from free carriers to bound pairs, $\eta_{\rm s}$ is the singlet exciton portion for fluorescence, $\eta_{\rm pl}$ is the photoluminescence quantum efficiency $\eta_{\rm pl} = \frac{k_{\rm r}}{k_{\rm r}+k_{\rm nr}}$ where $k_{\rm r(nr)}$ is the radiative (non-radiative) decay rate of the singlet exciton, and lastly $\eta_{\rm OC}$ is the optical coupling constant, namely the portion of generated photons escaping the device, which is typically around 0.2. The originality of Ma–Chi and Thompson–Forrest's work was to overcome the limit of singlet exciton only, namely, using electrophosphorescence to overcome the spin symmetry restriction, since the traditional wisdom stating the singlet exciton formation ratio is limited to 25% and the 75% triplet exciton is wasted. Strong spin–orbit coupling first converts singlet to triplet excited state and then coupled with the electric dipole interaction, the lowest triplet state continues to convert the excited-state energy to light. Such strategy can achieve 100% internal electroluminescence quantum efficiency [7], namely, all the injected electrons are converted to photons.

It can be noted that excited state, both electronic structure and dynamics, is the central theoretical

issue for organic light-emitting diodes (OLEDs), much as the band structure for inorganic semiconductors. In this review, for describing the (polymer) long-chain excited states, we developed symmetrized density matrix renormalization group (DMRG) for long-ranged potential to examine the excited-state orderings which governs the light emitting and is governed by electron correlation. For complex molecules such as organometallic and aggregation-induced emission (AIE) molecules, we applied the time-dependent density functional theory (TDDFT). For the excited-state dynamics, since the time scale spans from nanosecond to microsecond, we derived a vibration correlation function rate formalism to avoid the complexity of excited-state dynamics. And the center of focus is η_S and η_{pl}.

BREAKING THE CURSE OF 25% LIMIT FOR η_S IN OLEDS

Electrophosphorescence can lead to $\eta_S = 100\%$. However, triplet emission suffers from the TTA at high current density, causing a serious efficiency drooping. Moreover, triplet emission in general has long lifetime, detrimental for display technology. Seeking highly efficient singlet emission has been a longstanding task for OLEDs. Breaking the curse of 25% limit for η_S in OLEDs has long become the center of interest in the field. Along this line, Cao *et al.* demonstrated that for ordered large molecular weight polymers, the external electroluminescence quantum efficiency can reach 4% while that of photoluminescence is 8%, implying the possibility of singlet formation ratio exceeding the 25% spin statistical limit [8]. This finding has aroused very strong fundamental interest, not only for the sake of seeking highly efficient singlet emission materials, but also for the understanding of the elementary electronic processes in OLEDs. A variety of theoretical models have been proposed starting with Shuai *et al.* postulating a conjecture: $\eta_s = \frac{k_S}{k_S+3k_T}$ [9], where $k_{S(T)}$ is the singlet (triplet) exciton formation rate, followed by a number of arguments which all demonstrated the possibility of $k_S > k_T$ or even $k_S \gg k_T$ [10–14]. Such theoretical perspective stimulated further experimental explorations into the spin-dependent exciton formation dynamics which in general support the theoretical prediction [15–19]. One essential assumption in such a model is the diminishingly small exchange energy for the interchain charge transfer (CT) state (see Scheme 1), which allows facile interconversion between the singlet and triplet CT manifolds, as

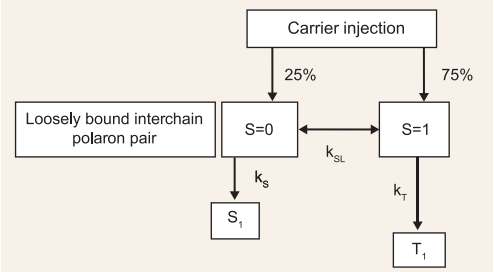

Scheme 1. Schematic sketch of the spin-dependent exciton formation process, where k_{SL} is the spin-lattice relaxation rate, usually much faster than both k_S and k_T. Once $k_S > k_T$, the spin statistics is beaten. Reproduced with permission from [27].

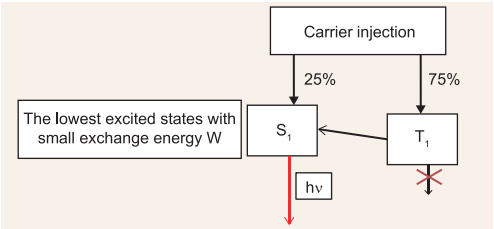

Scheme 2. Principle of TADF proposed by Adachi *et al.*

demonstrated experimentally for well-ordered ladder-type poly-paraphenylenes [20]. The eventual exciton formation rates from CT states are indeed spin dependent. And a simple form is postulated $r_{S/T} = \frac{k_S}{k_T} = \frac{E_b^T}{E_b^S}$ [21,22], where E_b is the exciton binding energy. We found that $r_{S/T}$ is electric field dependent [22] from quantum chemistry computation, which is confirmed by experiment only very recently: by virtue of the computed $r_{S/T}$, Takahashi *et al.* have directly monitored bias-dependent variations in the exciton formation ratio of working organic light-emitting diodes [23]. Successful proving of principle in materials design have also been achieved in Philips Research Center for polymer [24] and by a Michigan–Singapore collaboration in molecular design leading to a discovery of OLEDs materials with internal quantum efficiency from 40% to 62% [25,26].

Recently, Adachi *et al.* proposed the thermally activated delayed fluorescence (TADF) mechanism (see Scheme 2) by upconverting the electro-pumped triplets back to singlets, achieving $\eta_S = 100\%$ [28]. The difference between Scheme 1 and Scheme 2 is that the interchain process is not needed for the latter and the spin conversion now occurs at the lowest excited state with small exchange energy in donor–acceptor (D-A) molecules with minimum overlap between the highest occupied molecular orbital (HOMO) and the lowest unoccupied molecular orbital

(LUMO): the energy gap between S_1 and T_1 (twice the exchange energy) can be approximated as $2W = 2\int \psi_H(r_1)\psi_L(r_1)\frac{1}{r_{12}}\psi_H(r_2)\psi_L(r_2)dr_1dr_2$. For the D-A compounds, HOMO distributes mostly on donor part while LUMO on the spatially separated acceptor part, leading to a small W, then the electro-pumped triplets T_1 can easily be converted to S_1 through a thermally activated reverse intersystem crossing, resulting in delayed fluorescence and achieving in principle 100% singlet emission [29]. Since the electric transition dipole moment can be expressed as $\mu = e\int \psi_H(r)r\psi_L(r)dr$, it is immediately noted that the TADF compounds in general possess low radiative decay rate, which is proportional to μ^2. Thus, molecular design strategy needs to consider molecular packing mode to suppress the non-radiative decay channels. In addition, the efficiency roll-off becomes serious at high current due to the long delayed process.

An alternative way to beat the 25% statistic limit is to benefit the TTA which can convert partially electro-excited triplets back to singlet excited states, namely, two triplets recombine to generate one singlet, elevating the theoretical singlet portion limit to 25% + 75%/2 = 62.5%. Monkman *et al.* have demonstrated the working principle [30]. The advantage of TTA is to avoid the D-A type exciton, detrimental for charge recombination. In fact, an efficient TTA process is favored by a relatively large exchange energy W, allowing a large radiative decay rate. Nevertheless, TTA would also lead to more singlet ground states. It was estimated that only 15% can be added from triplet manifold to singlet excitons [31]. Thus, efficiency improvement from this approach is quite bounded.

Very recently, Ma *et al.* came up with a hot exciton mechanism, or hybridized local and charge transfer (HLCT) [32]. The central idea is to mix the localized excitation (LE) with the CT state in molecular design so that the CT excited states locate above the LE ones: the former is helpful for interconversion between spin manifolds, while the latter favor optical emission, shown in Scheme 3. This picture is also close to Scheme 1, except now all the energy levels stem from intramolecular species, instead of intermolecular one. These authors have demonstrated some successful molecular design examples, such as triphenylamine (TPA) substituted anthracene derivative, achieving 50% singlet exciton portion. Further developments based on TPA have produced high electroluminescence efficiency approaching 97% for singlet portion [33]. A novel bipolar phenanthroimidazole derivative has also been shown to yield singlet exciton portion of 31%, which was attributed to the HLCT mechanism by Lee *et al.* [34].

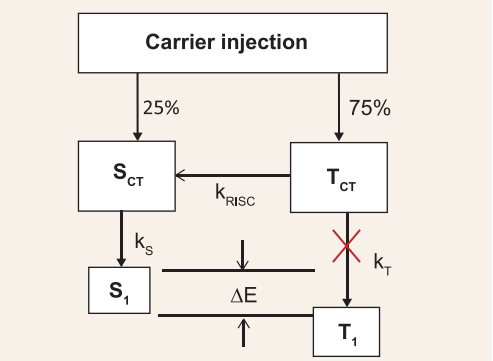

Scheme 3. Energy level diagram of hot exciton mechanism proposed by Ma *et al.*

Li *et al.* investigated the electroluminescence for neutral π-radicals [35]. The neutral radical itself possesses spin half. Combined with injected electron and hole, the three-spin system can give eight microstates with 4 states of spin 1/2 and 4 states of spin 3/2. So, intrinsically, even from the spin statistics, the internal quantum efficiency limit is 50% (not 100% as claimed in [35]). Denoting spin up as α and down as β, for two particles (electron and hole), we have the injected pair as

$$|S=0, S_z=0\rangle = \frac{1}{\sqrt{2}}[\alpha(1)\beta(2)-\alpha(2)\beta(1)] \quad (1)$$

$$\begin{aligned} |S=1, S_z=1\rangle &= \alpha(1)\alpha(2) \\ |S=1, S_z=0\rangle &= \frac{1}{\sqrt{2}}[\alpha(1)\beta(2)+\alpha(2)\beta(1)] \\ |S=1, S_z=-1\rangle &= \beta(1)\beta(2) \end{aligned} \quad (2)$$

Spin 1/2 (the radical) coupling with S = 0 gives rise to two microstates:

$$\begin{aligned} &\left|S=\frac{1}{2}, S_z=\frac{1}{2}\right\rangle \\ &\quad = \frac{1}{\sqrt{2}}[\alpha(1)\beta(2)-\alpha(2)\beta(1)]\alpha(3) \\ &\left|S=\frac{1}{2}, S_z=-\frac{1}{2}\right\rangle \\ &\quad = \frac{1}{\sqrt{2}}[\alpha(1)\beta(2)-\alpha(2)\beta(1)]\beta(3) \end{aligned} \quad (3)$$

And the coupling with S = 1 results in total spin 3/2 and 1/2. The former with four microstates is wasted since the initial state (radical) is spin 1/2, and the latter with two microstates can be written by virtue of

Clebsh–Gordon coefficients as:

$$\begin{aligned}\left|S=\frac{1}{2},S_z=\frac{1}{2}\right\rangle &= \sqrt{\frac{2}{3}}\alpha(1)\alpha(2)\beta(3) \\ &\quad -\sqrt{\frac{1}{6}}\left[\alpha(1)\beta(2)+\alpha(2)\beta(1)\right]\alpha(3) \\ \left|S=\frac{1}{2},S_z=-\frac{1}{2}\right\rangle &= \sqrt{\frac{1}{6}}\left[\alpha(1)\beta(2)+\alpha(2)\beta(1)\right]\beta(3) \\ &\quad -\sqrt{\frac{2}{3}}\beta(1)\beta(2)\alpha(3) \qquad (4)\end{aligned}$$

Thus, out of eight microstates, we get four spin conserved, $\eta_S = 50\%$.

Nevertheless, usually the molecular radical possesses low photoluminescence quantum efficiency. Even with higher spin statistical limit for electro-pumped excitation, the overall efficiency is low for radical. It is highly desirable to design radical with high photoluminescence. This is a new direction with potential application.

Li and Shuai *et al.* recently put forward a TPI (triplet-polaron interaction) mechanism to explain a highly efficient OLED materials 4-N-[4-(9-phenylcarbazole)]-3,5-bis(4-diphenlamin)phenyl-4*H*-1,2,4-triazole, for which the TADF, TTA, and HLCT mechanisms have been all carefully excluded [36]. The collision of a triplet exciton (S = 1) with a polaron (S = 1/2) can produce a singlet exciton (S = 0) and a polaron (S = 1/2), which is a spin-conserving process: $T + P^+ \rightarrow P^+ + S$. Since the triplet exciton is directly electro-excited, the collision with carrier can lead to direct emission, which is driven by thermal activation, electric field, as well as intermolecular electron or hole hopping. Energetically, this process is upconversion. However, two factors make this process possible: (i) theoretically, we demonstrated that this is a spin-allowed process and the electronic coupling term has the same origin as the intermolecular CT which is two to three orders of magnitude larger than the spin–orbit coupling required for intersystem crossing; (ii) due to the presence of polaron, the electric field can accelerate the process providing a favorable driving force.

In one word, the generally believed wisdom widely documented in textbook that the internal quantum efficiency for organic electrofluorescence is limited to 25% can be broken either through molecular design or by intermolecular organization.

THE ORDERINGS OF THE LOWEST LYING EXCITED STATES IN CONJUGATED CHAIN

Michael Kasha made an outstanding observation: the molecular luminescence is determined by the lowest excited state [37], termed as Kasha's rule. This became a principle for molecular design of luminescent materials, even though there exist exceptions such as azulene derivatives where optical emission was from the S_2 state [38]. Thus, molecule or polymer with a dipole-forbidden lowest excited state deems to be non-emissive. The first conducting polymer, polyacetylene, is dark due to the long known fact that the lowest excited state in polyene is of even parity A_g state. For polyene, the HOMO to LUMO transition (|H-L>) is always dipole allowed (B_u) state. However, due to the electron correlation effect, the lowest excitation in polyenes is no longer |H-L> transition. Instead, it is of double excitation |HH-LL>. This calls for accurate computational methodology for calculating the lowest lying excited-state structure. Even with the state-of-the-art TDDFT with commonly employed functionals, the lowest excited state is always computed to be of B_u symmetry, much as in single electron model. Other post-Hartree–Fock method is not applicable for large systems with high accuracy: it was demonstrated that even the equation-of-motion coupled cluster single and double (EOM/CCSD) method produced the wrong ordering for polyenes longer than 20 π-electrons [39]. Organic materials usually have quite low dielectric constant $\varepsilon \sim 2$–3, in contrast to inorganic semiconductor ($\varepsilon > 10$). Thus, in the solid state, the Coulomb interaction ($V(r) = \frac{1}{\varepsilon r}$) cannot be well screened out. For the optical property, such interaction leads to much more pronounced electron-hole binding, or exciton. And it is also the origin of the excited-state ordering alteration. The minimal model to describe electron correlation effect is the Hubbard model, which gives a penalty U in energy for double occupation. But this model is not appropriate for exciton, since the Hubbard U does not contain any attraction between electron and hole at half-filling [40,41]. In fact, in the occupation representation, an electron excitation is a double occupation site and a hole is the empty site. In the large *U* limit, the charge excitation energy is simply *U-4t* both for infinite electron-hole separation (band edge) and for finite separation (exciton), leading to zero exciton binding. Once a nearest-neighbor correlation term *V* is introduced, the smallest nearest neighbor excitation energy becomes *U-V-2t,* leading to an exciton binding energy *V-2t* [41]. In addition, to distinguish the chemical difference for the polymer unit cell, we add another parameter δ designated as the bond-alternation

parameter. So, the model Hamiltonian for the conjugated chain reads:

$$H = -\sum_i t[1+(-1)^i\delta](c_{i\sigma}^{+}c_{i+1\sigma} + h.c.) + U\sum_i n_{i\uparrow}n_{i\downarrow} + V\sum_i (n_i-\mu)(n_{i+1}-\mu) \quad (5)$$

where t and V are the nearest neighbor transfer integral and Coulomb interaction, respectively, δ is the bond length alternation parameter, and μ is the chemical potential. Such model can indeed correctly describe the exciton binding behavior for conjugated polymer [40,41]. The V-term is a simplified Pariser–Parr–Pople long-range potential $\sum_{i<j} V(r_{ij})(n_i-\mu)(n_j-\mu)$, a semi-empirical quantum chemistry model.

White proposed the DMRG formalism which was found to be almost exact for short-ranged 1D quantum systems, such as Heisenberg model and Hubbard model [42]. The reduced density matrix for the *i*th iteration is obtained from the ground-state wavefunction of the (*i-1*)th step and is continuously truncated to a fixed space dimension. For shorted-ranged 1D model, the reduced density matrix is quite localized. However, the accuracy drastically decreases even going to 2D localized system such as t-J model [43]. In addition, since the reduced density matrix depends on the targeted state, excited state usually expands in different reduced Hilbert space from the ground state, which needs different algorithm. Our symmetrization algorithm [44] as well as the extension to long-ranged potential [45,46] has been shown to give reliable descriptions for conjugated chain systems for the low-lying excited-state ordering, the exciton binding energy which has been hotly debated for polymers [40,46], and the nonlinear optical response [47], for all of which electron correlation effect is shown dominates. These work, especially the extension to long-range potential started the application of DMRG to quantum chemistry. Thanks to the eminent contributions by Chan [48], DMRG now becomes an option for highly accurate quantum chemistry calculation [49]. It is especially powerful when coupled with traditional post-Hartree–Fock methods [50,51].

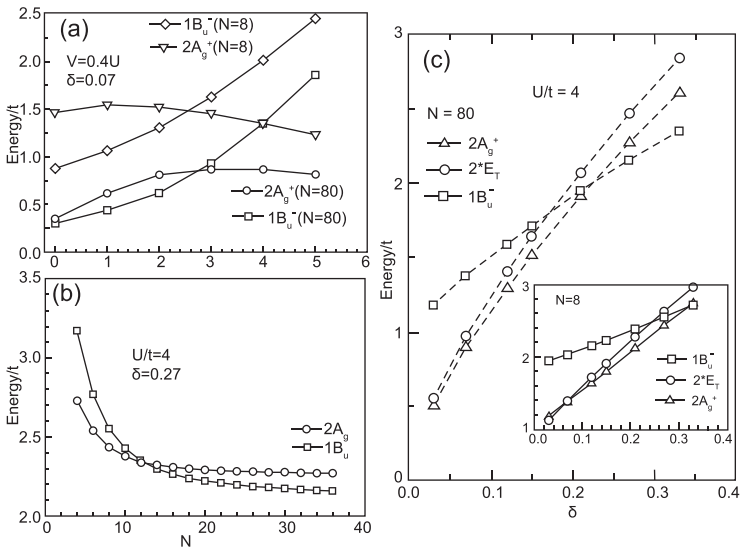

Figure 1. $1B_u$ and $2A_g$ with respect to Hubbard U (a) and DMRG reveals excited-state ordering as a function of (b) chain length and (c) bond length alternation. Reprinted with permission from [45]. © 1997 by the International Society for Optical Engineering.

For the model Hamiltonian (Equation 5), a symmetrization scheme based on center inversion, charge conjugation, and spin flip (for half-filling) was found to be highly effective for targeting the low-lying excited states for conjugated long chains. Spin flip symmetry helps to divide the basis into odd (S = 1, 3, 5,…) and even (S = 0, 2, 4,…) space, thus excluding the triplet excitation from the singlet manifold. Charge conjugation operation interchanges electron and hole at half-filling, classifying the excitation space into 'covalent' and 'ionic' subspaces. This symmetry is especially useful when optical excitation is concerned since the selection rule requires the electric dipole transition occur between covalent and ionic states. The advantage of such symmetrization lies in automatically excluding the intruding configurations in the renormalization processes.

The ordering of the low-lying excited states is sensitive to many factors, especially the electron correlation and electron–phonon coupling. It was long known that in poylenes, the excitation with double excitation character ($2A_g$) lies below the single excitation ($1B_u$), in sharp contrast to the mean-field description. Such behavior is illustrated in Fig. 1a for model system of Equation (5) for N = 8 and N = 80 calculated by our symmetrized DMRG. It showed that electron correlation tends to enhance the ionic excitation and to stabilize the covalent excitation.

Further investigations demonstrated more excited-state ordering crossovers. Soos *et al.* first pointed out an effective bond length alternation crossover [52]. Later, we found that the crossover point is also size dependent, implying possibility of a quantum confinement effect for the ordering [45]. The DMRG nearly exact solutions present two kinds of crossovers shown in Fig. 1b and c.

Fig. 1b implies that for some parameter for short conjugated chain, if $2A_g$ is below $1B_u$, upon elongating the chain length, the $1B_u$ can become below, since $2A_g$ can be viewed as two triplet states, which

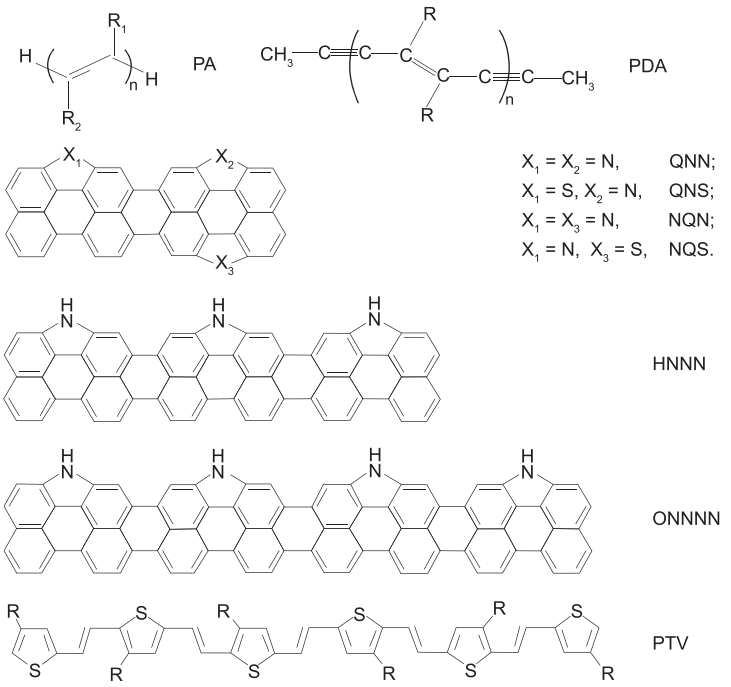

Scheme 4. Chemical structures of the derivatives of PA, PDA, rylenes, and PTV.

is repulsive when chain is too short, but when the space is allowed, the $2A_g$ state saturates since triplets are much more localized than $1B_u$ state. Fig. 1c indicated that for short chain ($N = 8$), the critical δ is around 0.27 but for long chain, it becomes 0.15. This implies that for δ between them, there should occur N crossover as in Fig. 1b.

The excited-state ordering crossover can be employed for molecular design. It is known that both polyacetylene (PA) and polydiacetylene (PDA) are dark because their $2A_g$ is below $1B_u$ but PDA possesses large carrier mobility (chemical structure see Scheme 4). The question is how to make chemical substitutions to alter the ordering so that PA or PDA can emit light. This is possible in principle. Since the $1B_u$ is of ionic character, if the chemical substitution can induce CT from side group to the backbone to stabilize the lowest ionic excited state, then $1B_u$ can come below $2A_g$. Since the ordering is very sensitive to the levels of theory, it is impossible even nowadays to carry out highly accurate quantum chemistry method to decide the excited-state ordering for large systems. Based on our basic understandings and some benchmark calculations, we came up with a quantity ρ to characterize the amount of charge transferred from side chain to backbone $\rho = \frac{\sum_{\mu\in \mathrm{sub}} |C_{H\mu}|^2}{\sum_{\mu\in \mathrm{sub}} |C_{L\mu}|^2}$, where $C_{H(L)\mu}$ is the molecular orbital coefficient of HOMO (LUMO) at the polymer backbone adjacently linking to the substituents [53]. The assumption behind is that, in general, the ionic $1B_u$ state can be simply described by a single determinant excitation HOMO → LUMO. If ρ is close to 1.00, it implies that the chemical substitutes contribute equally to HOMO and LUMO, thus does not change the nature of excitation. Suppose ρ deviates well away from 1.00, it means some imbalance between electron and hole upon substitution, implying possibility of ionic character is enforced. ρ can be easily calculated from molecular orbital theory such as Hartree–Fock or DFT, instead of highly time consuming or even impossible correlated electronic structure methods which is necessary for $2A_g$.

For PA, we list in Table 1 the molecular orbital calculation results with various substituents, in comparison with the experiments. It is seen that the ρ value correlates well with the luminescence behavior: namely, for ρ is well away from 1, luminescence of the substituted PA is strong.

Unfortunately, for PDA with a series of substituents, the ρ values are always around 1. The preliminary investigation indicated that it is impossible to make PDA light emitting. To reveal the difference between PA and PDA, we depict the frontier orbital profiles upon substitution in Fig. 2. The charge distributions spread to the side chain (phenyl rings) for PA but not for PDA, since the latter can be regarded as more 'rigid' electronically: namely, side-chain substitution cannot alter the frontier orbital in the polymer backbone.

Next example is the molecular design for highly efficient red or infrared emission molecules: narrow gap implies small radiative decay rate and large internal conversion rate according to the energy gap law. We predicted a series of red and near infrared strongly emitting rylene derivatives by introducing heteroatom bridges into the dark long-chain rylenes [57]. The optical properties of rylenes have attracted

Table 1. Calculated ρ values from the optimized geometry at B3LYP/6-31G level for disubstituted PA.

R_1	H	H	Ethyl	Ethyl	Ethyl	Ph
R_2	Ph	Ethyl	Ph	4-(Methoxycarbonl)phenyl)	4-Benzoyl phenyl	Ph
ρ	0.91	1.21	0.60	8.47	0.29	0.43
Emission	Weak[a]	Weak[a]	Strong[b]	Strong[b]	Strong[b]	Strong[b,c]

[a]From [54]. [b]From [55]. [c]From [56].

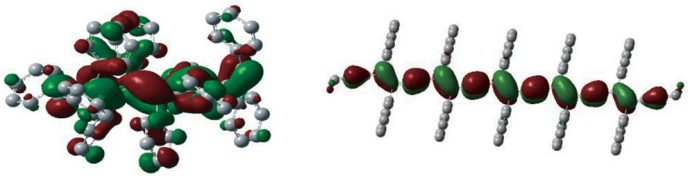

Figure 2. HOMO of substituted (a) PA and (b) PDA. Reprinted with permission from [53]. © 2006 by the World Scientific Publishing Company.

considerable attention because it is very facile to gain the emissions in full color range by solely changing the chain length [58]. But it is unfortunate the dark $2A_g/B_{3g}$ state lies below $1B_u$ state when the chain length is elongated to some extent. The crossover of $1B_u/2A_g$ occurs between terrylene and quaterylene according to quantum chemistry calculation at various levels. Consequently, the perylene and terrylene emit strong fluorescence while the quaterrylene and longer rylenes show much weaker or undetectable fluorescence as observed in experiments [59,60]. Following the molecular design rule based on the quantity ρ, we try to vary the frontier orbital nature by introducing the electron-withdrawing heteroatom bridges along the side chain (seen in Scheme 4).

The calculated ρ values as well as the lowest excited singlet state property are listed in Table 2, and all deviated appreciably from 1.0 for the rylene derivatives, because the annulated heteroatoms can indeed cause the charge redistribution of the frontier orbitals as expected. Namely, the LUMO orbitals delocalized over the heteroatoms owing to their electron-withdrawing ability while the HOMO orbitals are unchanged for not involving the contribution of heteroatoms (taking QNN as an example compared with the pristine quaterrylene seen in Fig. 3). The emission spectra and quantum efficiencies are further predicted in Fig. 4. And they are found to be the desiring excellent red and near-infrared emitters with maximum peak position at 670–1008 nm and large fluorescent quantum yield over 90%.

Another application for molecular design is for the photovoltaic polymers. Poly(3-hexylthiophene) is a landmark materials but the power conversion efficiency is limited by the relatively large band gap. Poly(2,5-thienylene vinylene) (PTV) and its derivatives (Scheme 4) possess low bandgap 1.55–1.8 eV and large carrier mobility [61 and 62]. Surprisingly, the photovoltaic performance is extremely low (0.2%–0.9%) [63]. Ultrafast spectroscopy for a PTV oligomer: PCBM composite by Heeger group demonstrated that the photoinduced electron transfer efficiency is as low as 5% and the non-radiative decay time is as short as 0.6 ps [64]. Namely, PTV is non-emissive. It was suggested that there exists concomitant relationship between light emitting and photovoltaics, the two completely inverse processes. In fact, Li group found that the photovoltaic efficiency for the non-emissive P3HTV is as low as 0.2%. However, upon chemical substitution, the emissive poly(3-carboxylated-2,5-thienylene vinylene), it reaches 2% [65]. This is

Table 2. Calculated ρ from the DFT optimized geometry for the X-annulated rylenes, in comparison with the MRCI/ZINDO results for S_1. NA stands for not available.

Compounds	Quaterrylene	QNN	QNS	NQN	NQS	HNNN	ONNNN
ρ	1.0	2.54	2.30	1.85	1.70	2.46	2.45
S_1	$2A_g$	1B	$1B_u$	A′	A′	NA	NA
Emission	Weak[a]	Strong	Strong	Strong	Strong	Strong	Strong

[a]From [60].

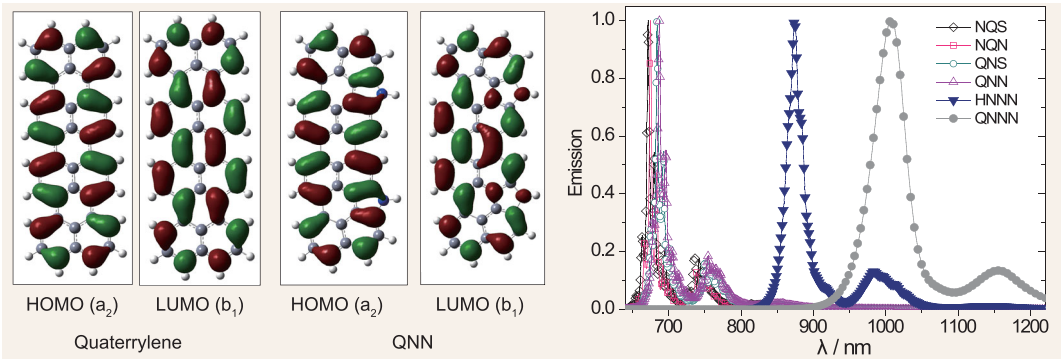

Figure 3. Molecular orbitals of Quaterrylene and QNN, and the emission spectra of the designed molecules NQS, NQN, QNS, QNN, HNNN, and ONNNN.

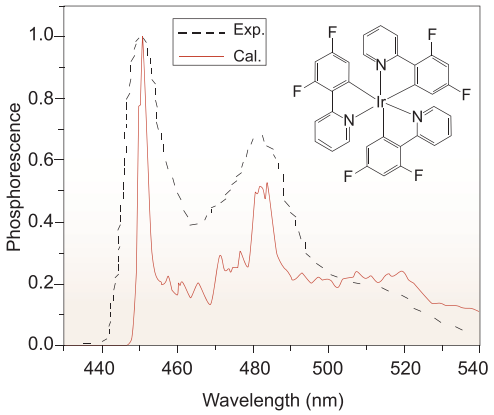

Figure 4. Theoretical and experimental phosphorescence emission spectra at 77 K. Reprinted with permission from [76]. © 2013 by the Chinese Chemical Society.

understandable from the exciton diffusion point of view: supposing the photoexcitation is relaxed to the lowest state $2A_g$, it can no longer migrate through dipole–dipole interaction.

High-level quantum chemical calculation indicated that $2A_g$ is below $1B_u$ for pristine PTV [66]. Molecular orbital calculations for the ρ values of the five-type substitutions are given in Table 3 in comparison with the nature of S_1 and experimental luminescence. It is seen indeed when ρ is close to 1.00, there is no luminescence. The computational study not only reproduces well the experimental facts that no luminescence for CH_3 or OH substitution and with luminescence for COOH, but also predicts two compounds with electron withdrawing groups CHO and NO_2 could be emissive, thus potential candidate for photovoltaic application.

FORMALISM FOR EVALUATING THE NON-RADIATIVE DECAY RATE AND THE LUMINESCENCE QUANTUM EFFICIENCY

Now, we come to the photoluminescence quantum efficiency $\eta_{\rm pl} = \frac{k_r}{k_r+k_{\rm nr}}$. k_r is dictated by spontaneous emission mainly determined by the Einstein relationship $k_{\rm r} = f\Delta E^2/1.5$, where f is the dimensionless oscillator strength and ΔE is the vertical transition energy (in unit of $\rm cm^{-1}$) at the excited-state geometry to give rise to the rate in unit of $\rm s^{-1}$. When line-width broadening effect due to vibrational regression is considered, the rate can be obtained by integration over the whole emission spectrum: $k_{\rm r} = \int {\rm d}\omega\sigma_{\rm emi}(\omega)$. For most organic chromophores, $f \sim 1.0$, and for visible light, the typical radiative decay rate is between 10^8 and 10^9 $\rm s^{-1}$. Namely, the time scale for OLEDs is nanosecond for fluorescence. This poses a serious challenge for theoretical investigation on the non-radiative decay process, since the molecular dynamics involving the excited state can only be run up to picosecond scale, far shorter than the light-emitting process. Thus, the rate assumption from the Fermi–Golden rule is practically the only way to computationally assess the $\eta_{\rm pl}$. In such an approach, the nuclear motion can be considered as a collection of harmonic oscillators. Even for complex molecules, the Franck–Condon factor as well as the Herzberg–Teller effect and the Duschinsky rotation effect (DRE) can be taken into account to evaluate the optical absorption and emission spectra as well as to calculate the radiative decay rate at the first-principles level now [67–72]. The major difficulty to estimate $\eta_{\rm pl}$ lies in the non-radiative decay. $k_{\rm nr}$ consists of two contributions: the internal conversion $k_{\rm IC}$ from S_1 to S_0 and the intersystem crossing $k_{\rm ISC}$ from S_1 to T_1 arising from the non-adiabatic coupling and spin–orbit coupling, respectively:

$$\hat{H}'\Psi_{{\rm i}v_{\rm i}} = \hat{H}^{\rm BO}\Phi_{\rm i}(\mathbf{r};\mathbf{Q})\Theta_{{\rm i}v_{\rm i}}(\mathbf{Q}) + \hat{H}^{\rm SO}\Phi_{\rm i}(\mathbf{r};\mathbf{Q})\Theta_{{\rm i}v_{\rm i}}(\mathbf{Q}) \quad (6)$$

where $\hat{H}^{\rm BO}$ is the non-adiabatic coupling and $\hat{H}^{\rm SO}$ is the spin–orbit coupling, $\mathbf{r}$ and $\mathbf{Q}$ are the electronic and nuclear normal coordinates, respectively, and Φ and Θ are the wavefunctions for electron and vibrational motions, respectively. By neglecting the small term $\partial^2\Phi_i/\partial Q_{fl}^2$, the first term can be expressed as

$$\begin{aligned}&\left\langle \Phi_{\rm f}\Theta_{{\rm f}v_{\rm f}} \left| \hat{H}^{\rm BO} \right| \Phi_{\rm i}\Theta_{{\rm i}v_{\rm i}} \right\rangle \\ &= -\hbar^2 \sum_k \left\langle \Phi_{\rm f}\Theta_{{\rm f}v_{\rm f}} \left| \frac{\partial\Phi_i}{\partial Q_{fk}} \frac{\partial\Theta_{{\rm i}v_{\rm i}}}{\partial Q_{fk}} \right\rangle \right. \\ &= \sum_k \left\langle \Phi_{\rm f}\Theta_{{\rm f}v_{\rm f}} \left| \left(\hat{P}_{fk}\Phi_{\rm i}\right)\left(\hat{P}_{fk}\Theta_{{\rm i}v_{\rm i}}\right) \right\rangle \right. \end{aligned} \quad (7)$$

P_k is the nuclear momentum operator for the kth normal mode, index f is the final electronic state. For the internal conversion process, the transition

Table 3. Calculated ρ from the DFT optimized geometry for different substituted OTVs, in comparison with the MRCI/ZINDO results for S_1. NA stands for not available.

−R	−H	$-CH_3$	−OH	−COOH	$-NO_2$	−CHO
ρ	1.29	1.2	0.91	1.51	1.4	1.85
S_1	$2A_g$	$2A_g$	$2A_g$	$1B_u$	$1B_u$	$1B_u$
Emission	No	No	No	Yes	NA	NA

rate can be recast as

$$k_{\mathrm{IC}} = \frac{2\pi}{\hbar}\sum_{v_\mathrm{i},v_\mathrm{f}} P_{iv_\mathrm{i}}(T)\left|\sum_k \langle\Phi_\mathrm{f}|\hat{P}_k|\Phi_\mathrm{i}\rangle \times \left\langle\Theta_{\mathrm{f}v_\mathrm{f}}\left|\hat{P}_k\right|\Theta_{iv_\mathrm{i}}\right\rangle\right|^2 \delta\left(E_{iv_\mathrm{i}} - E_{\mathrm{f}v_\mathrm{f}}\right) \quad (8)$$

Where P_i is the statistical averaged weight of the initial state.

Under the harmonic oscillator model and the Condon approximation, by virtue of Fourier transformation for the Dirac delta function, the rate can be reduced to

$$k_{\mathrm{IC}} = \frac{1}{\hbar^2}\int_{-\infty}^{\infty} \mathrm{d}t\, \mathrm{e}^{\mathrm{i}\omega_{\mathrm{if}}t}\sum_{k,l} Z_\mathrm{i}^{-1} R_{kl}\rho_{\mathrm{IC},kl}(t,T) \quad (9)$$

where $R_{kl} = \langle\Phi_\mathrm{f}|\hat{P}_{\mathrm{f}k}|\Phi_\mathrm{i}\rangle\langle\Phi_\mathrm{i}|\hat{P}_{\mathrm{f}l}|\Phi_\mathrm{f}\rangle$ is the non-adiabatic electronic coupling prefactor and Z_i is the partition function. $\rho_{IC,kl}(t,T)$ is the thermal vibrational correlation function, first obtained by Peng *et al.* [73]:

$$\rho_{IC,kl}(t,T) = \mathrm{Tr}\left[\hat{P}_{\mathrm{f}k}e^{-i\tau_\mathrm{f}\hat{H}_\mathrm{f}}\hat{P}_{\mathrm{f}l}e^{-i\tau_\mathrm{i}\hat{H}_\mathrm{i}}\right] \quad (10)$$

We fist trace over the initial (excited) state nuclear coordinates:

$$\rho_{\mathrm{IC},kl}(t,T) = \int_{-\infty}^{\infty} d\underline{x}'\left\langle\underline{x}'\left|\hat{P}_{\mathrm{f}k}e^{-i\tau_\mathrm{f}\hat{H}_\mathrm{f}}\hat{P}_{\mathrm{f}l}e^{-i\tau_\mathrm{i}\hat{H}_\mathrm{i}}\right|\underline{x}'\right\rangle \quad (11)$$

where the vector $\underline{x}'$ represents the excited-electronic (initial) state normal mode coordinates Q_{e_j}. Inserting three complete sets of ground (final) states $\underline{y}$, $\underline{z}$, and $\underline{w}$, and one complete set of the excited (initial) states $\underline{y}'$:

$$\begin{aligned}\rho_{\mathrm{IC},kl}(t,T) = \int_{-\infty}^{\infty} dx\,dy\,dz\,dw\,dx'\,dy' &\times\langle x'\,|\,x\rangle\langle x|\hat{P}_{\mathrm{f}k}|y\rangle \\ &\times\langle y|e^{-i\tau_\mathrm{f}\hat{H}_\mathrm{f}}|z\rangle\langle z|\hat{P}_{\mathrm{f}l}|w\rangle\langle w|y'\rangle \\ &\times\langle y'|e^{-i\tau_\mathrm{i}\hat{H}_\mathrm{i}}|x'\rangle\end{aligned} \quad (12)$$

The transformation between two spaces is the Duschinsky rotation:

$$\langle\underline{x}'\,|\,\underline{x}\rangle = \delta[\underline{x}' - (S\underline{x} + \underline{D})] \quad (13)$$

And the normal momentum matrix element is

$$\langle x_k|\,\hat{P}_{\mathrm{f}k}\,|y_k\rangle = -\mathrm{i}\hbar\frac{\partial}{\partial x_k}\delta(x_k - y_k) \quad (14)$$

By virtue of multidimensional Gaussian integration of the type:

$$\langle x|\,e^{-i\tau H}\,|y\rangle = \sqrt{\frac{a(\tau)}{2\pi i\hbar}} \times \exp\left\{\frac{i}{\hbar}\left[\frac{1}{2}b(\tau)(x^2+y^2) - a(\tau)xy\right]\right\} \quad (15)$$

for harmonic oscillator Hamiltonian H, where $a(\tau) = \omega/\sin(\hbar\omega\tau)$ and $b(\tau) = \omega/\tan(\hbar\omega\tau)$, Equation (12) can be integrated analytically after some extremely tedious algebra, see [74]. Due to the mathematical analyticity, the computational scale is simply N^3 before entering Equation (9) for time integration, which can be computed efficiently through fast Fourier transformation technique.

The spin–orbit coupling brings about three major effects: (i) the intersystem crossing from S_1 to T_1 non-radiatively, which adds to k_{nr} in the denominator for determining the photoluminescence efficiency; (ii) the phosphorescence from T_1 to S_0 via one virtual electric dipole transition step; (iii) and the direct non-radiative decay from T_1 to S_0 to compete with the phosphorescence. Parallel to Equations (9–12), the three decay rates related to transitions across spin manifolds can be also expressed analytically, see [75]. Namely, we have five rates formalisms expressed by thermal vibration correlation function at the same footings: displaced and distorted harmonic oscillator model.

We took *fac*-tris(2-(4,6-difluorophenyl)pyridyl iridium (*fac*-Ir(F_2ppy)$_3$) as an example to investigate its photophysical properties by the above formalisms [76]. Fluorination in the ligand led to a blueshift in emission compared to the archetype *fac*-Ir(ppy)$_3$. The geometry optimization for S_0 and T_1 has been carried out by B3LYP and UB3LYP – 6–31G** with Ir with LANL2DZ basis, respectively.

Based on the S_0 structure, the spin–orbit coupling constants are calculated by the Dalton program and the non-adiabatic coupling coefficient is evaluated by a first-order perturbation. First, we compared our theoretical phosphorescence spectrum with experiment from [77] in Fig. 4, where only 0.1 eV shift in origin was made to match the peaks, well justifying the applicability of UB3LYP for the triplet state. There is no broadening factor introduced: the spectrum lineshape is simply from the vibronic structure and temperarature effect.

Table 4. Photophysical properties of *fac*-Ir(F_2ppy)$_3$ at 298 K.

	λ_{max}(nm)	Φ_p	k_r (s^{-1})	k_{nr} (s^{-1})
Cal.	470.44	0.73	2.69×10^5	1.00×10^5
Exp.[a]	466	0.98	5.8×10^5	1.2×10^4
Exp.[b]	469	0.77	4.7×10^5	1.4×10^5
Exp.[c]	468	0.43	2.7×10^5	3.6×10^5

[a]In 2-MeTHF solution, [77]. [b]In 2-MeTHF glass, [78]. [c]In CH_2Cl_2, [79].

The spin–orbit coupling between T_1 and S_0 is calculated to be 61 cm^{-1}, by averaging the three components of T_1 microstates. The calculated radiative and non-radiative decay rates at 298 K are listed in Table 4, in comparing with the experiments. Note that the theoretical values are calculated in gas phase. The comparison with the measurements is quite satisfactory since there is no free adjustable parameter in such formalism.

THEORETICAL INVESTIGATION OF THE AIE PHENOMENA

Now, we focus on the application of the above formalism to understand the exotic AIE phenomena. It was known for a long time that photoluminescence is often quenched with increasing chromophore concentration [80,81]. Even though intermolecular electron delocalization might increase the electric transition dipole moment or oscillator strength enhancing the radiative decay rate, there are a variety of reasons to counteract to cause luminescence quenching, among which are (i) the intermolecular charge separation (or electron transfer) making radiative recombination more difficult; (ii) the intermolecular energy transfer to traps or quenching sites; and especially, (iii) the Davidov splitting making the lower energy state component with reduced oscillator strength (H-type aggregate). According to Birks, many aromatic luminophores emit strongly as isolated molecules, but suffer from concentration quenching due to the intermolecular π-π interaction [80,81]. There exist certain cases with aggregation enhanced emission, for instance the J-aggregate where the lowest exciton state concentrates all the oscillator strength, largely enhancing the radiative decay rate and allowing possibility of superradiation [82]. But that requires long-range order which is often difficult for organic crystals, let alone for thin film with amorphous packings. That is why the concept proposed in 2001 by Tang *et al.* of the AIE [83] has continuously attracted intensive research [84]. Similar photophysical behavior had been reported for electron withdrawing substituted oligophenylenevinylenes [85]. The systematic exploration and amplified investigation and application of such exotic phenomena have led to better understanding of the mechanism which turned out to be insightful for molecular design [86].

For the OLEDs application, the device is in solid state. AIE becomes one of the molecular design strategies searching for highly efficient light-emitting materials. It has also become an effective way to detect the concentration effect for application in bio- or chemico-sensing. Several possible AIE mechanisms have been proposed, including the restriction of intramolecular rotations [87,88], J-aggregation formation [89,90], excimer formation [91], intramolecular planarization [92], twisting intramolecular CT [93], and hydrogen-bonding [94]. Intermolecular interaction has a complicated impact on the photophysics for the aggregates. We tackle the AIE issue by quantitatively computing the radiative and non-radiative decay rates for molecule in gas phase or solution and in aggregate, to look at the environment effect on both the radiative and non-radiative decay rates. We first take the AIE star molecule silole (1,1,2,3,4,5-hexaphenylsilole, HPS) as example, see Fig. 5a.

The solid-state luminescence quantum efficiency of HPS is measured as high as 78% in thin film, 260-fold increase compared with that (0.3%) in cyclohexane [95]. We build a cluster cut from the X-ray molecular crystal structure to mimic the solid-state environment effect. The computational study was carried out by the hybrid quantum mechanics and molecular mechanics (QM/MM) approach. The computational model of HPS set up is showed in Fig. 5b, which includes one central QM molecule, active MM-part with 11 nearest molecules, and frozen MM part with 63 molecules. The (TD)-B3LYP/6-31G(d) and the general Amber force field were adopted for QM and MM parts, respectively, in Chemshell package interfacing TURBOMOLE and DL-POLY programs. In addition, the molecule in solution was simply treated as in gas phase because the experimental measurements were operated in the extremely dilute non-polar solution. More computational details can be found in [96].

The aggregation effect on molecular structures is observed through comparing the modifications between the S_0 and S_1 states in gas phase with those in solid phase. Upon excitation, the main

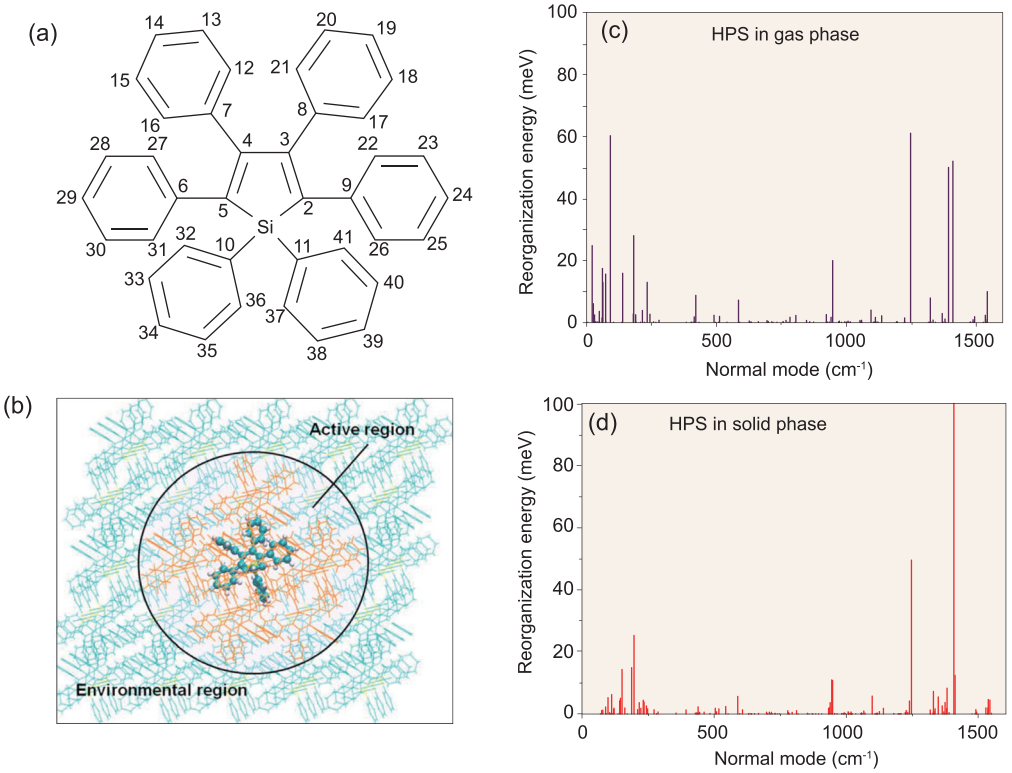

Figure 5. (a) Molecular structure of HPS with labels, (b) computational QM/MM model for HPS, and the reorganization energy versus normal modes of HPS in gas phase (c) and solid phase (d). Reprinted with permission from [92]. © 2013 by the American Chemical Society.

modifications appear in the dihedral angles between the central silacycle and the peripheral phenyl rings (especially the phenyl rings at 2,5-positions). The rotational motions of the peripheral phenyl rings around the Si-C bond in gas phase are much freer than those in solid. And the resulting modifications of D(Si-C2-C9-C26) and D(Si-C5-C6-C31) between the S_0 and S_1 states in gas phase are 14.56° and 14.63°, respectively, much larger than the counterparts 5.85° and 1.05° in solid phase.

Table 5 lists the calculated radiative and non-radiative decay rates of HPS in gas and solid phases. As expected, the non-radiative decay rate decreases by four orders of magnitude from 3.76×10^{11} s^{-1} in gas phase to 2.06×10^{7} s^{-1} in solid phase. While the radiative decay rate is insensitive to the aggregation environment. Consequently, the solid-state quantum efficiency is far higher than that in gas phase, which is in good agreement with the experimental result. More interestingly, it is also found in Table 5 that if the DRE is neglected, the non-radiative decay rate would be $\sim 10^5$ s^{-1} and hardly varies from gas to solid phases, which is much smaller than the radiative decay rate of $\sim 10^7$ s^{-1}. This is in contrast to the fact that there is no emission in solution. Therefore, the DRE is very important to account for the excited-state decay rate for the AIEgens.

DRE is a parameter to directly measure the mixing degree of different normal modes during the transition process. Generally, the low-frequency normal modes possess strong DRE. From the reorganization energies decomposition into normal mode relaxation for HPS in gas and solid phases shown in Fig. 5c and d, it can be seen that many low-frequency normal modes with wavenumber less than 100 cm^{-1} are active in gas phase while much fewer modes taking part in solid phase.

The reorganization energy dictates the Franck–Condon factor [97]. It characterizes the ability of accepting the excited-state energy transformed into heat, from which we can analyze the contribution of every normal mode to the non-radiative decay rate. Comparing the reorganization energies of HPS molecule in gas phase and in cluster in Fig. 5c and d, it is found that in gas phase many low-frequency normal modes (<100 cm^{-1}) take charge of the dominant non-radiative decay channels as well as a few high-frequency normal modes. While in solid state the channels of low-frequency modes are blocked largely and only the high-frequency modes are unswervingly

Table 5. Calculated k_r and k_{IC} of HPS in gas and solid phases at room temperature. 'No DRE' means without considering DRE.

	k_r (s^{-1})		k_{IC} (s^{-1})	
	DRE	No DRE	DRE	No DRE
Gas	1.05×10^7	4.76×10^7	3.76×10^{11}	6.65×10^5
Solid	6.56×10^7	6.53×10^7	2.06×10^7	9.36×10^5

responsible for the non-radiative decay. These important low-frequency normal modes belong to the rotational/twisting vibrations of the peripheral phenyl rings around the Si-C bond, which just corresponds to the significant modifications of geometries between S_0 and S_1 states described above. The high-frequency normal modes are the stretching vibration of C-C bonds in silacycle, which is requisite for emission of an organic lumophore. Thus, from solution to solid phases, the low-frequency rotational/twisting vibrations are largely suppressed from the surrounding molecular interaction and the non-radiative decay channels are considerably blocked. This sharply decreases the non-radiative decay rate, which cannot compete with the radiative decay. Thus, the strong fluorescence is induced by aggregation.

In order to reveal the AIE mechanism in a more explicit way, we proposed to use the resonance Raman spectroscopy (RRS) to unravel the aggregation effect on the non-radiative decay process. The RRS cross-section reads

$$\sigma \propto \omega_I {\omega_S}^3 \frac{|\mu_0|^4 \omega_j \lambda_j}{2(\omega_{eg} - \omega_I)^4}$$
$$\Rightarrow \sigma \propto \omega_j \lambda_j \Rightarrow \sigma/\omega_j \propto \lambda_j \quad (16)$$

Thus, the RRS intensity is proportional to the product of the reorganization energy and the frequency for every normal mode. More detailed derivations can be found in [98,99].

We choose a typical AIEgen 1,2-Diphenyl-3,4-bis(diphenylmethylene)-1-cyclobutene (HPDMCb) and a non-AIEgen 2,3-dicyanopyrazino phenanthrene (DCPP) to probe the aggregation effect on their non-radiative decay rates. First, we investigated the radiative and non-radiative decay rates of the two compounds in solution and in solid phases by using the approaches mentioned above. As expected, the non-radiative decay rate of HPDMCb is reduced by four orders of magnitude from 1.31×10^{11} s^{-1} in solution to 2.29×10^7 s^{-1} in solid phase, while the radiative decay rate is blunt to the change of environment. Thus, the AIE behavior of HPDMCb is well reproduced. Different from HPDMCb, both the radiative and non-radiative decay rates of DCPP are insensitive to the aggregation, $\sim 10^6$ s^{-1}. Through analyzing the reorganization energy feature of both compounds given in Fig. 6, we found that the reorganization energy of low-frequency normal modes in HPDMCb significantly drops from solution to solid phases because the modes are largely restricted, while the reorganization energy feature in DCPP is similar in the two phases.

Figure 6 shows the calculated RRS for HPDMCb and DCPP in solution and in solid phases. For HPDMCb, there are remarkable blueshift (>40 cm^{-1}) in the low-frequency region and slight hypsochromic shift (<20 cm^{-1}) in high-frequency region from solution to solid phase. Moreover, the RRS intensities of the low-frequency normal modes with respect to the high-frequency ones sharply decrease from solution to solid state. The feature of RRS just corresponds to that of the reorganization energy in Fig. 6 as expected. The low-frequency modes of 24, 51, and 78 cm^{-1} with strong RRS signals in solution and the one of 70 cm^{-1} corresponding to the first RRS peak in solid phase are all the out-of-plane torsional/twisting motions of the peripheral phenyl rings. These results indicate that the low-frequency torsional/twisting motions of HPS are very active in solution but become inert owing to the surrounding molecular interaction in solid phase. On the other hand, for DCPP, the whole RRS lineshape is quite similar in the two phases and the RRS signal starts to appear at the region of >200 cm^{-1}. This suggests that there is no low-frequency mode involved in the transition process and the relevant high-frequency modes are not affected by the aggregation.

SUMMARY AND OUTLOOK

Massive scale OLEDs application just starts now for consumable products. Even larger application in flexible display and solid-state lighting is foreseeable. Seeking highly efficient organic emitters is still an ongoing research hot spot. In this review, we have emphasized three aspects relating to OLEDs from theoretical and computational perspectives. First, we have discussed the longstanding efforts to beat the curse for organic materials for the internal quantum efficiency limit of 25% from the spin statistics.

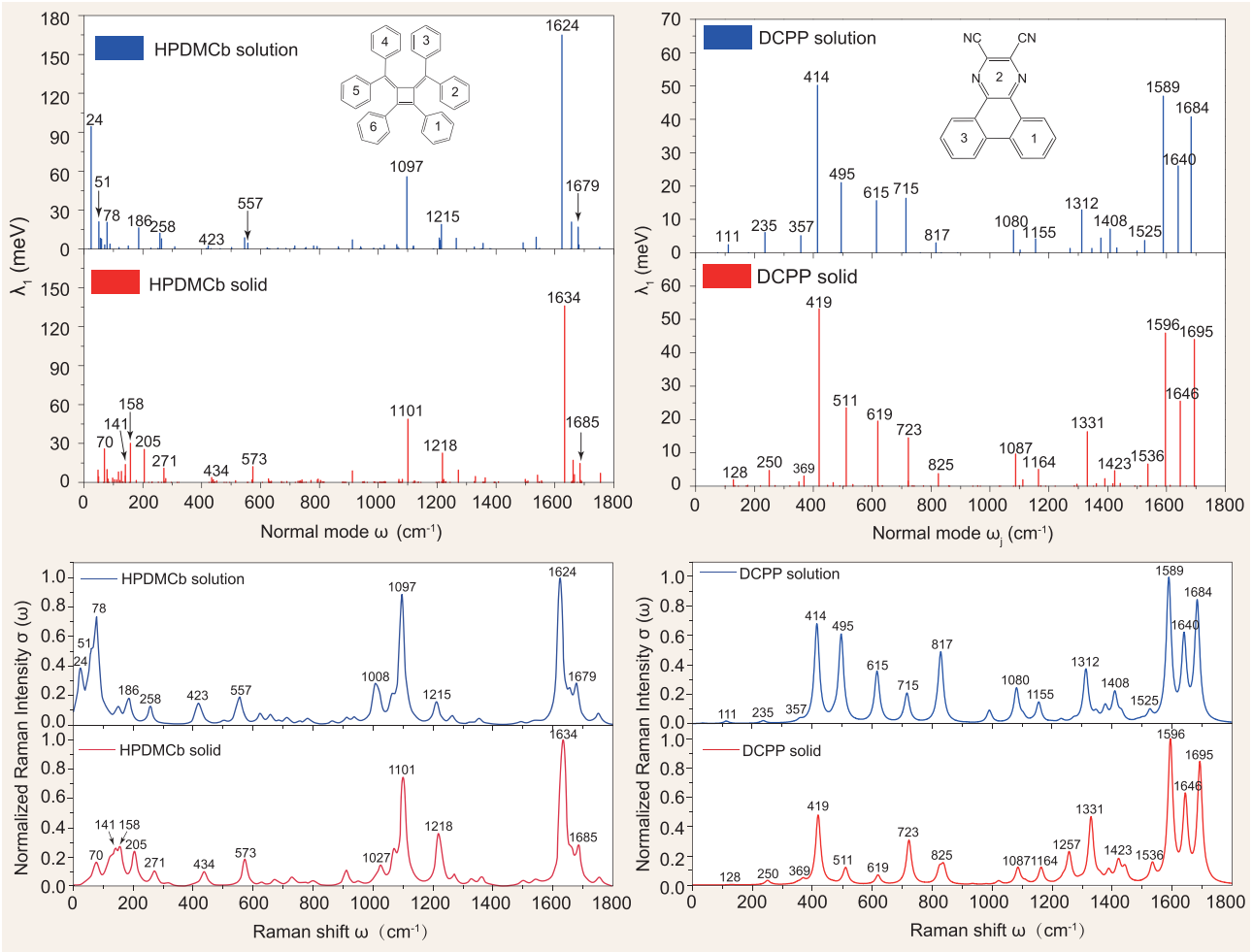

Figure 6. The reorganization energy λ_j versus the normal modes of HPDMCb and HPS in solution and solid phases (top) and the RRS intensity σ of HPDMCb and DCPP in solution and solid phases (bottom). Reprinted with permission from [99]. © 2015 by the American Chemical Society.

Through assuming an intermediate interchain CT state, we found that such limit can be beaten up by spin-dependent exciton formation rates. We also reviewed recent advances in TADF, TTA, hot exciton, neutral radicals, and even triplet–polaron interaction. All these indicate the 25% limit for OLEDs can be broken. These investigations pointed out the importance of intermediate state for the excited-state dynamics, which has been overlooked for functional materials but well known for catalytic process, namely, the transition state. From our earlier interchain CT state, to the recent intramolecular high-lying CT state in the hot-exciton model, the exciton formation via intermediate state is clearly demonstrated. More photophysical investigations are called up. And which mechanism can survive the commercial application is still unclear. Second, we discussed the nature of the lowest excited state, with its symmetry and oscillator strength, dictating optical emissions. The electronic excited state remains a major challenge in computational chemistry, especially when the multireference contribution is important, for example the $2A_g$ state. EOM-CCSD is in general believed to be highly accurate and reliable. However, we found it failed to describe relatively large active space. The ordering is so much sensitive to theoretical treatment on electron correlation. The efforts to understand the low-lying excited state in extended conjugated chain had led to the application of DMRG in quantum chemistry, which now become a main stream highly accurate method for correlated electron systems. Third, we pointed out that the dynamics simulation for electronic process requires a time step in the order of attosecond, and for nuclear motion, of femtosecond, while the radiative decay time is typically around nanosecond, or even micro- or milli-seconds for phosphorescence, leading to the impracticability of the nonadiabatic dynamics simulation. We thus proposed a rate formalism to capture the essential quantum feature of nuclear vibration at the level of harmonic oscillator. Such an approach needs inputs

from standard quantum chemistry package providing molecular parameters such as ground state and excited-state vibrational modes and vibronic couplings, the non-adiabatic coupling and spin–orbit coupling, etc. It indeed gave satisfactory results for both the optical spectra and the radiative and non-radiative decay rates, for both organic molecules and organometallics, justifying the applicability for modeling OLEDs materials. When such formalism is coupled with QM/MM scheme, the molecular aggregate effect on light emitting can be understood quantitatively. The AIE phenomena are revealed through computational study and a plausible way to probe the microscopic mechanism is proposed. The mega challenges in theoretical chemistry lies in the excited-state dynamics for complex system for long time behavior. In one word, both electron correlation effect and electron-nuclear coupled dynamics are essential for understanding OLEDs. These just happen to be at the core of theoretical chemistry, which is far from a ready-made tool for molecular design of highly efficient materials.

ACKNOWLEDGEMENTS

Contributions from the following collaborators are greatly acknowledged: Shiwei Yin, Liping Chen, Yuqian Jiang, Tian Zhang, Jean-Luc Brédas, David Beljonne, Surja Ramasesha, and Swapan Pati.

FUNDING

This work was supported by the National Natural Science Foundation of China (21290190) and the National Basic Research Program of China (2013CB834703 and 2015CB655002).

REFERENCES

1. Tang CW and Vanslyke SA. Organic electroluminescent diodes. *Appl Phys Lett* 1987; **51**: 913–5.
2. Burroughes JH, Bradley DDC and Brown AR *et al.* Light-emitting-diodes based on conjugated polymers. *Nature* 1990; **347**: 539–41.
3. Gustafsson G, Cao Y and Treacy GM *et al.* Flexible light-emitting-diodes made from soluble conducting polymers. *Nature* 1992; **357**: 477–9.
4. Ma YG, Zhang HY and Shen JC *et al.* Electroluminescence from triplet metal-ligand charge-transfer excited state of transition metal complexes. *Synth Met* 1998; **94**: 245–8.
5. Baldo MA, O'Brien DF and You Y *et al.* Highly efficient phosphorescent emission from organic electroluminescent devices. *Nature* 1998; **395**: 151–4.
6. Burn PL, Lo SC and Samuel IDW. The development of light-emitting dendrimers for displays. *Adv Mater* 2007; **19**: 1675–88.
7. Adachi C, Baldo MA and Thompson ME *et al.* Nearly 100% internal phosphorescence efficiency in an organic light-emitting device. *J Appl Phys* 2001; **90**: 5048–51.
8. Cao Y, Parker ID and Yu G *et al.* Improved quantum efficiency for electroluminescence in semiconducting polymers. *Nature* 1999; **397**: 414–7.
9. Shuai Z, Beljonne D and Silbey RJ *et al.* Singlet and triplet exciton formation rates in conjugated polymer light-emitting diodes. *Phys Rev Lett* 2000; **84**: 131–4.
10. Tandon K, Ramasesha S and Mazumdar S. Electron correlation effects in electron-hole recombination in organic light-emitting diodes. *Phys Rev B* 2003; **67**: 045109.
11. Kobrak MN and Bittner ER. Quantum molecular dynamics study of polaron recombination in conjugated polymers. *Phys Rev B* 2000; **62**: 11473–86.
12. Hong TM and Meng HF. Spin-dependent recombination and electroluminescence quantum yield in conjugated polymers. *Phys Rev B* 2001; **63**: 075206.
13. Karabunarliev S and Bittner ER. Spin-dependent electron-hole capture kinetics in luminescent conjugated polymers. *Phys Rev Lett* 2003; **90**: 057402.
14. Ye A, Shuai ZG and Bredas JL. Coupled-Cluster approach for studying the singlet and triplet exciton formation rates in conjugated polymer Led's. *Phys Rev B* 2002; **65**: 045208.
15. Ho PKH, Kim JS and Burroughes JH *et al.* Molecular-scale interface engineering for polymer light-emitting diodes. *Nature* 2000; **404**: 481–4.
16. Wohlgenannt M, Tandon K and Mazumdar S *et al.* Formation cross-sections of singlet and triplet excitons in pi-conjugated polymers. *Nature* 2001; **409**: 494–7.
17. Wilson JS, Dhoot AS and Seeley A *et al.* Spin-dependent exciton formation in pi-conjugated compounds. *Nature* 2001; **413**: 828–31.
18. Dhoot AS, Ginger DS and Beljonne D *et al.* Triplet formation and decay in conjugated polymer devices. *Chem Phys Lett* 2002; **360**: 195–201.
19. Virgili T, Cerullo G and Luer L *et al.* Understanding fundamental processes in poly(9,9-dioctylfluorene) light-emitting diodes via ultrafast electric-field-assisted pump-probe spectroscopy. *Phys Rev Lett* 2003; **90**: 247402.
20. Kadashchuk A, Vakhnin A and Blonski I *et al.* Singlet-triplet splitting of geminate electron-hole pairs in conjugated polymers. *Phys Rev Lett* 2004; **93**: 066803.
21. Chen LP, Zhu LY and Shuai ZG. Singlet–triplet splittings and their relevance to the spin-dependent exciton formation in light-emitting polymers: an EOM/CCSD study. *J Phys Chem A* 2006; **110**: 13349–54.
22. Yin SW, Chen LP and Xuan PF *et al.* Field effect on the singlet and triplet exciton formation in organic/polymeric light-emitting diodes. *J Phys Chem B* 2004; **108**: 9608–13.
23. Takahashi T, Kanemoto K and Kanenobu M *et al.* Direct monitoring of bias-dependent variations in the exciton formation ratio of working organic light emitting diodes. *Sci Rep* 2015; **5**: 15533.
24. Meulenkamp EA, van Aar R and Bastiaansen JJAM *et al.* High-efficiency polymer LEDs: triplets and novel devices. *Proc SPIE—Int Soc Opt Eng* 2004; **5464**: 90–103.
25. Zhen CG, Chen ZK and Liu QD *et al.* Fluorene-based oligomers for highly efficient and stable organic blue-light-emitting diodes. *Adv Mater* 2009; **21**: 2425–9.

26. Zhen CG, Dai YF and Zeng WJ *et al.* Achieving highly efficient fluorescent blue organic light-emitting diodes through optimizing molecular structures and device configuration. *Adv Funct Mater* 2011; **21**: 699–707.
27. Shuai Z. Advances in theory for organic functional materials. In: Zhu DB (ed.). *Advances in Functional Materials* (in Chinese). Beijing: Chemical Industry Press, 2005.
28. Uoyama H, Goushi K and Shizu K *et al.* Highly efficient organic light-emitting diodes from delayed fluorescence. *Nature* 2012; **492**: 234–8.
29. Hirata S, Sakai Y and Masui K *et al.* Highly efficient blue electroluminescence based on thermally activated delayed fluorescence. *Nat Mater* 2015; **14**: 330–6.
30. King SM, Cass M and Pintani M *et al.* The contribution of triplet-triplet annihilation to the lifetime and efficiency of fluorescent polymer organic light emitting diodes. *J Appl Phys* 2011; **109**: 074502.
31. Wallikewitz BH, Kabra D and Gélinas S *et al.* Triplet dynamics in fluorescent polymer light-emitting diodes. *Phys Rev B* 2012; **85**: 045209.
32. Li WJ, Pan YY and Xiao R *et al.* Employing ∼100% excitons in OLEDs by utilizing a fluorescent molecule with hybridized local and charge-transfer excited state. *Adv Funct Mater* 2014; **24**: 1609–14.
33. Zhang ST, Yao L and Peng QM *et al.* Achieving a significantly increased efficiency in nondoped pure blue fluorescent OLED: a quasi-equivalent hybridized excited state. *Adv Funct Mater* 2015; **25**: 1755–62.
34. Chen M, Yuan Y and Zheng J *et al.* Novel bipolar phenanthroimidazole derivative design for a nondoped deep-blue emitter with high singlet exciton yields. *Adv Opt Mater* 2015; **3**: 1215–9.
35. Peng QM, Obolda A and Zhang M *et al.* Organic light-emitting diodes using a neutral pi radical as emitter: the emission from a doublet. *Angew Chem-Int Ed* 2015; **54**: 7091–5.
36. Obolda A, Peng QM and He CY *et al.* Triplet-polaron interaction induced upconversion from triplet to singlet: a possible way to obtain highly efficient OLEDs. *Adv Mater* 2016; **28**: 4740–6.
37. Kasha M. Characterization of electronic transitions in complex molecules. *Discuss Faraday Soc* 1950; **9**: 14–9.
38. Beer M and Longuet-Higgins HC. Anomalous light emission of Azulene. *J Chem Phys* 1955; **23**: 1390–1.
39. Shuai Z and Brédas JL. Coupled-cluster approach for studying the electronic and nonlinear optical properties of conjugated molecules. *Phys Rev B* 2000; **62**: 15452–60.
40. Shuai Z, Pati SK and Su WP *et al.* Binding energy of 1Bu singlet excitons in the one-dimensional extended Hubbard-Peierls model. *Phys Rev B* 1997; **55**: 15368–71.
41. Shuai Z, Brédas JL and Pati SK *et al.* Exciton binding energy in the strong correlation limit of conjugated chains. *Phys Rev B* 1998; **58**: 15329–32.
42. White SR and Martin R. Ab initio quantum chemistry using the density matrix renormalization group. *J Chem Phys* 1999; **110**: 4127–30.
43. White SR and Scalapino DJ. Density matrix renormalization group study of the striped phase in the 2D t–J model. *Phys Rev Lett* 1998; **80**: 1272–5.
44. Ramasesha S, Pati SK and Krishnamurthy HR *et al.* Symmetrized density-matrix renormalization-group method for excited states of Hubbard models. *Phys Rev B* 1996; **54**: 7598–601.
45. Shuai Z, Brédas JL and Pati SK *et al.* Quantum-confinement effects on the ordering of the lowest-lying excited states in conjugated polymer. *Proc SPIE—Int Soc Opt Eng* 1997; **3145**: 293–302.
46. Yaron D, Moore EE and Shuai Z *et al.* Comparison of density matrix renormalization group calculations with electron-hole models of exciton binding in conjugated polymers. *J Chem Phys* 1998; **108**: 7451–8.
47. Shuai Z, Brédas JL and Saxena A *et al.* Linear and nonlinear optical response of polyenes: a density matrix renormalization group study. *J Chem Phys* 1998; **109**: 2549–55.
48. Chan GK-L and Sharma S. The density matrix renormalization group in quantum chemistry. *Annu Rev Phys Chem* 2011; **62**: 465–81.
49. Hedegård ED, Knecht S and Kielberg JS *et al.* Density matrix renormalization group with efficient dynamical electron correlation through range separation. *J Chem Phys* 2015; **142**: 224108.
50. Kurashige Y, Chalupsky J and Lan TN *et al.* Complete active space second-order perturbation theory with cumulant approximation for extended active-space wavefunction from density matrix renormalization group. *J Chem Phys* 2014; **141**: 174111.
51. Sharma S and Alavi A. Multireference linearized coupled cluster theory for strongly correlated systems using matrix product states. *J Chem Phys* 2015; **143**: 102815.
52. Soos ZG, Ramasesha S and Galvao DS. Band to correlated crossover in alternating Hubbard and Pariser-Parr-Pople chains – nature of the lowest singlet excitation of conjugated polymers. *Phys Rev Lett* 1993; **71**: 1609–12.
53. Chen L, Hou X and Zhu L *et al.* Theoretical design of light-emitting polymers – substitution effects of excited state ordering of polydiacetylene and polyacetylene. *J Theor Comput Chem* 2006; **5**: 391–400.
54. Turki M, Barisien T and Bigot J-Y *et al.* Excited states dynamics of polydiacetylenes: an ab initio and femtosecond spectroscopic investigation of the change from the acetylenic to the butatrienic structure. *J Chem Phys* 2000; **112**: 10526–37.
55. Sugita A and Kobayashi T. Dynamics of a photo-excited state in polydiacetylene studied by femtosecond mid-infrared absorption spectroscopy. *Chem Phys Lett* 2001; **346**: 41–6.
56. Manaka T, Yamada T and Hoshi H *et al.* Observation of the lowest Ag excited state lying in the optical gap in polydiacetylene by means of second-harmonic generation spectroscopy. *Synth Met* 1998; **95**: 155–8.
57. Peng Q, Niu Y and Wang Z *et al.* Theoretical predictions of red and near-infrared strongly emitting X-annulated rylenes. *J Chem Phys* 2011; **134**: 074510.
58. Grimsdale AC and Müllen K. The chemistry of organic nanomaterials. *Angew Chem Int Ed* 2005; **44**: 5592–629.
59. Sonnenschein M, Amirav A and Jortner J. Absolute fluorescence quantum yields of large molecules in supersonic expansions. *J Phys Chem* 1984; **88**: 4214–8.
60. Koch KH and Müllen K. Polyarylenes and poly(arylenevinylene)s, V. Synthesis of tetraalkyl-substituted oligo(1,4-naphthylene)s and cyclization to soluble oligo(peri-naphthylene)s. *Chem Ber* 1991; **124**: 2091–100.
61. Fuchigami H, Tsumura A and Koezuka H. Polythienylenevinylene thin-film transistor with high carrier mobility. *Appl Phys Lett* 1993; **63**: 1372–4.
62. Videlot C, Ackermann J and Blanchard P *et al.* Field-effect transistors based on oligothienylenevinylenes: from solution π-dimers to high-mobility organic semiconductors. *Adv Mater* 2003; **15**: 306–10.
63. Hou J, Tan Z and He Y *et al.* Branched poly(thienylene vinylene)s with absorption spectra covering the whole visible region. *Macromolecules* 2006; **39**: 4657–62.
64. Hwang IW, Xu QH and Soci C *et al.* Ultrafast spectroscopic study of photoinduced electron transfer in an oligo(thienylenevinylene): fullerene composite. *Adv Funct Mater* 2007; **17**: 563–8.
65. Huo L, Chen TL and Zhou Y *et al.* Improvement of photoluminescent and photovoltaic properties of poly(thienylene vinylene) by carboxylate substitution. *Macromolecules* 2009; **42**: 4377–80.

66. Jiang Y, Peng Q and Gao X *et al*. Theoretical design of polythienylenevinylene derivatives for improvements of light-emitting and photovoltaic performances. *J Mater Chem* 2012; **22**: 4491–501.
67. Yan YJ and Mukamel S. Eigenstate-free, green function, calculation of molecular absorption and fluorescence line shapes. *J Chem Phys* 1986; **85**: 5908–23.
68. Ianconescu R and Pollak E. Photoinduced cooling of polyatomic molecules in an electronically excited state in the presence of Dushinskii rotations. *J Phys Chem A* 2004; **108**: 7778–84.
69. He Y and Pollak E. Theory of cooling of room temperature benzene upon photoexcitation to the S_1 state. *J Phys Chem A* 2001; **105**: 10961–6.
70. Niu Y, Peng Q and Deng C *et al*. Theory of excited state decays and optical spectra: application to polyatomic molecules. *J Phys Chem A* 2010; **114**: 7817–31.
71. Borrelli R, Capobianco A and Peluso A. Generating function approach to the calculation of spectral band shapes of free-base chlorin including Duschinsky and Herzberg–Teller effects. *J Phys Chem A* 2012; **116**: 9934–40.
72. Santoro F, Lami A and Improta R *et al*. Effective method for the computation of optical spectra of large molecules at finite temperature including the Duschinsky and Herzberg-Teller effect: the Q(x) band of porphyrin as a case study. *J Chem Phys* 2008; **128**: 224311.
73. Peng Q, Yi Y and Shuai Z *et al*. Excited state radiationless decay process with Duschinsky rotation effect: formalism and implementation. *J Chem Phys* 2007; **126**: 114302.
74. Niu Y, Peng Q and Shuai Z. Promoting mode free formalism for excited state radiationless decay process with Duschinsky rotation effect. *Sci China Ser B-Chem* 2008; **51**: 1153–8.
75. Peng Q, Niu Y and Shi Q *et al*. Correlation function formalism for triplet excited state decay: combined spin-orbit and nonadiabatic couplings. *J Chem Theory Comput* 2013; **9**: 1132–43.
76. Shi QH, Peng Q and Sun SR *et al*. Vibration correlation function investigation on the phosphorescence quantum efficiency and spectrum for blue phosphorescent Ir(III) complex. *Acta Chim Sin* 2013; **71**: 884–91.
77. Sajoto T, Djurovich PI and Tamayo AB *et al*. Temperature dependence of blue phosphorescent cyclometalated Ir(III) complexes. *J Am Chem Soc* 2009; **131**: 9813–22.
78. Tamayo AB, Alleyne BD and Djurovich PI *et al*. Synthesis and characterization of facial and meridional tris-cyclometalated iridium(III) complexes. *J Am Chem Soc* 2003; **125**: 7377–87.
79. Dedeian K, Shi J and Shepherd N *et al*. Photophysical and electrochemical properties of heteroleptic tris-cyclometalated iridium(III) complexes. *Inorg Chem* 2005; **44**: 4445–7.
80. Förster T and Kasper K. Ein konzentrationsumschlag der fluoreszenz. des pyrens. *Z Elektrochem* 1955; **59**: 976–80.
81. Birks JB. *Photophysics of Atomatic Molecules*. London: John Wiley & Sons Ltd, 1973.
82. Gross M and Haroche S. Superradiance: an essay on the theory of collective spontaneous emission. *Phys Rep* 1982; **93**: 301–96.
83. Luo JD, Xie ZL and Lam JWY *et al*. Aggregation-induced emission of 1-methyl-1,2,3,4,5-pentaphenylsilole. *Chem Commun* 2001; **18**: 1740–1.
84. Mei J, Leung NLC and Kwok RTK *et al*. Aggregation-induced emission: together we shine, united we soar! *Chem Rev* 2015; **115**: 11718–940.
85. Oelkrug D, Tompert A and Gierschner J *et al*. Tuning of fluorescence in films and nanoparticles of oligophenylenevinylenes. *J Phys Chem B* 1998; **102**: 1902–7.
86. Hong YN, Lam JWY and Tang BZ. Aggregation-induced emission. *Chem Soc Rev* 2011; **40**: 5361–88.
87. Hong YN, Lam JWY and Tang BZ. Aggregation-induced emission: phenomenon, mechanism and applications. *Chem Commun* 2009; 4332–53.
88. Mei J, Hong YN and Lam JWY *et al*. Aggregation-induced emission: the whole is more brilliant than the parts. *Adv Mater* 2014; **26**: 5429–79.
89. An BK, Kwon SK and Jung SD *et al*. Enhanced emission and its switching in fluorescent organic nanoparticles. *J Am Chem Soc* 2002; **124**: 14410–5.
90. Choi S, Bouffard J and Kim Y. Aggregation-induced emission enhancement of a meso-trifluoromethyl BODIPY via J-aggregation. *Chem Sci* 2014; **5**: 751–5.
91. Liu Y, Tao X and Wang F *et al*. Intermolecular hydrogen bonds induce highly emissive excimers: enhancement of solid-state luminescence. *J Phys Chem C* 2007; **111**: 6544–9.
92. Sonoda Y, Tsuzuki S and Goto M *et al*. Fluorescence spectroscopic properties of nitro-substituted diphenylpolyenes: effects of intramolecular planarization and intermolecular interactions in crystals. *J Phys Chem A* 2010; **114**: 172–82.
93. Hu R, Lager E and Aguilar-Aguilar A *et al*. Twisted intramolecular charge transfer and aggregation-induced emission of BODIPY derivatives. *J Phys Chem C* 2009; **113**: 15845–53.
94. Xiao S, Zou Y and Wu J *et al*. Hydrogen bonding assisted switchable fluorescence in self-assembled complexes containing diarylethene: controllable fluorescent emission in the solid state. *J Mater Chem* 2007; **17**: 2483–9.
95. Yu G, Yin SW and Liu YQ *et al*. Structures, electronic states, photoluminescence, and carrier transport properties of 1,1-disubstituted 2,3,4,5-tetraphenylsiloles. *J Am Chem Soc* 2005; **127**: 6335–46.
96. Zhang T, Jiang Y and Niu Y *et al*. Aggregation effects on the optical emission of 1,1,2,3,4,5-hexaphenylsilole (HPS): a QM/MM study. *J Phys Chem A* 2014; **118**: 9094–104.
97. Lin SH, Chang CH and Liang KK *et al*. Ultrafast dynamics and spectroscopy of bacterial photosynthetic reaction centers. *Adv Chem Phys* 2002; **121**: 1–88.
98. Ma HL, Liu J and Liang WZ. Time-dependent approach to resonance Raman spectra including Duschinsky rotation and Herzberg-Teller effects: formalism and its realistic applications. *J Chem Theory Comput* 2012; **8**: 4474–82.
99. Zhang T, Ma HL and Niu YL *et al*. Spectroscopic signature of the aggregation-induced emission phenomena caused by restricted nonradiative decay: a theoretical proposal. *J Phys Chem C* 2015; **119**: 5040–7.